J. Fluid Mech. (2012), *vol.* 692, *pp.* 317–331. © Cambridge University Press 2012
doi:10.1017/jfm.2011.514

Stressed horizontal convection

J. Hazewinkel[1], F. Paparella[2]† and W. R. Young[1]

[1] Scripps Institution of Oceanography, La Jolla CA 92093-0213, USA

[2] Department of Mathematics, University of Salento, Lecce 73100, Italy

(Received 26 July 2011; revised 1 October 2011; accepted 15 November 2011;
first published online 5 January 2012)

We consider the problem of a Boussinesq fluid forced by applying both non-uniform temperature and stress at the top surface. On the other boundaries the conditions are thermally insulating and either no-slip or stress-free. The interesting case is when the direction of the steady applied surface stress opposes the sense of the buoyancy driven flow. We obtain two-dimensional numerical solutions showing a regime in which there is an upper cell with thermally indirect circulation (buoyant fluid is pushed downwards by the applied stress and heavy fluid is elevated), and a second deep cell with thermally direct circulation. In this two-cell regime the driving mechanisms are competitive in the sense that neither dominates the flow. A scaling argument shows that this balance requires that surface stress vary as the horizontal Rayleigh number to the three-fifths power.

Key words: buoyant boundary layers, ocean circulation, ocean processes

1. Introduction

In 1908, Sandström began his work on horizontal convection with the remark: 'The motive for these experiments was the following observation I made at the Bornö station in the Gullmarfjord on the west coast of Sweden. When the wind swept over the fjord, the water at the surface flowed in the direction of the wind. Yet, as soon as the wind ceased, it flowed back in the opposite direction.' For an English translation of Sandström's paper, and the history of the horizontal-convection problem, see Kuhlbrodt (2008).

Horizontal convection is convection generated by imposing non-uniform buoyancy along a horizontal surface (Stern 1975). The problem has attracted considerable attention due to the suggestion of Munk & Wunsch (1998) that mechanical energy sources – such as the wind stress observed by Sandström (1908) – are necessary to sustain the ocean circulation. Recent work on horizontal convection is reviewed by Hughes & Griffiths (2008). Despite Sandström's pioneering recognition of the importance of surface wind stress, there has been only a little discussion of the interaction between imposed surface stress with surface buoyancy forcing within the context of horizontal convection. An early exception is the study by Beardsley & Festa (1972). More recently Ilicak & Vallis (2011) have examined the effect of an oscillatory surface stress on horizontal convection. In this paper we revisit the surface-stress

† Email address for correspondence: wryoung@ucsd.edu

https://doi.org/10.1017/jfm.2011.514 Published online by Cambridge University Press

problem formulated by Beardsley & Festa (1972) with greater computational resources, and with an improved understanding of horizontal convection.

The point of Munk & Wunsch (1998) regarding energy sources can be appreciated by considering the mechanical energy budget of horizontal convection (Paparella & Young 2002). Consider a three-dimensional rotating fluid in a rectangular box and represent the density as $\rho = \rho_0(1 - g^{-1}b)$, where b is the 'buoyancy'. The Boussinesq equations of motion are then

$$\frac{\mathrm{D}\boldsymbol{u}}{\mathrm{D}t} + 2\boldsymbol{\Omega} \times \boldsymbol{u} + \boldsymbol{\nabla} p = b\hat{\boldsymbol{z}} + \nu\nabla^2\boldsymbol{u}, \tag{1.1}$$

$$\frac{\mathrm{D}b}{\mathrm{D}t} = \kappa\nabla^2 b, \tag{1.2}$$

$$\boldsymbol{\nabla} \cdot \boldsymbol{u} = 0. \tag{1.3}$$

The kinematic viscosity is ν and the thermal diffusivity is κ. The boundary conditions on the velocity $\boldsymbol{u} = (u, v, w)$ are $\boldsymbol{u} \cdot \hat{\boldsymbol{n}} = 0$, where $\hat{\boldsymbol{n}}$ is the outward normal. The vertical coordinate is $-H < z < 0$. At the top surface, $z = 0$, the boundary conditions are

$$b = b_s(x, y) \quad \text{and} \quad \nu u_z\hat{\boldsymbol{x}} + \nu v_z\hat{\boldsymbol{y}} = \boldsymbol{\tau}_s(x, y); \tag{1.4}$$

the surface buoyancy b_s and surface stress $\boldsymbol{\tau}_s$ are prescribed with $0 \leqslant b_s(x, y) \leqslant b_{max}$ and $0 \leqslant |\boldsymbol{\tau}_s(x, y)| \leqslant \tau_{max}$. There is no flux of heat through the bottom, $z = -H$, or through the sidewalls. The viscous boundary conditions on the bottom and sidewalls are some combination of no-slip and no-stress.

We denote the total volume and time average by angular brackets $\langle\rangle$. Thus, the average mechanical energy dissipation is

$$\varepsilon \stackrel{def}{=} \nu\langle|\boldsymbol{\nabla} u|^2 + |\boldsymbol{\nabla} v|^2 + |\boldsymbol{\nabla} w|^2\rangle. \tag{1.5}$$

(The contents of $\langle\rangle$ above differ from the local dissipation by a divergence term with zero volume integral.) Taking the dot product of the momentum equation in (1.1) with $\boldsymbol{u}$ and averaging over the volume, one has

$$\varepsilon = \langle wb\rangle + H^{-1}\,\overline{\boldsymbol{u}_s \cdot \boldsymbol{\tau}_s}, \tag{1.6}$$

where $\boldsymbol{u}_s \stackrel{def}{=} \boldsymbol{u}(x, y, 0, t)$ is the surface velocity and the overbar denotes an average over x, y and t. This shows that the viscous dissipation ε is balanced by the conversion of potential energy into kinetic energy via the correlation in $\langle wb\rangle$ and by the stress work $\overline{\boldsymbol{\tau}_s \cdot \boldsymbol{u}_s}$. In Sandström's observation the wind is doing net positive work because the surface velocity is in the direction of the wind, i.e. $\overline{\boldsymbol{\tau}_s \cdot \boldsymbol{u}_s} > 0$. However, if the surface velocity is against the direction of the wind, then the atmosphere is extracting energy from the ocean.

Taking the (x, y, t)-average of (1.2), and using the no-flux condition at $z = -H$, one has

$$\overline{wb} - \kappa\bar{b}_z = 0. \tag{1.7}$$

Thus there is no net vertical buoyancy flux through every level $z =$ constant. The 'zero-flux' constraint (1.7) is a distinctive feature of horizontal convection, and remains in force when the problem is enriched by the addition of either surface stress forcing $\boldsymbol{\tau}_s$ or an interior body force (Tailleux & Rouleau 2010). Another expression for the buoyancy flux $\langle wb\rangle$ in (1.6) is obtained by averaging (1.7) over z:

$$\langle wb\rangle = \frac{\kappa\,\Delta\bar{b}}{H}, \tag{1.8}$$

https://doi.org/10.1017/jfm.2011.514 Published online by Cambridge University Press

where $\Delta\bar{b} \equiv \bar{b}(0) - \bar{b}(-H)$ is the difference between the horizontally averaged buoyancy at the top and bottom of the box.

The role of available potential energy in horizontal convection has recently been examined by several authors (Hughes, Hogg & Griffiths 2009; Tailleux 2009; Winters & Young 2009). Relevant to this discussion is that $\langle wb \rangle$ is the net rate of transfer between available potential energy and kinetic energy, and also the conversion between total potential energy and kinetic energy. Thus (1.8) provides a restrictive bound on conversions between kinetic and both forms of potential energy.

Eliminating the buoyancy flux $\langle wb \rangle$ between (1.6) and (1.8), one then has

$$H\varepsilon = \kappa \Delta\bar{b} + \overline{\boldsymbol{\tau}_s \cdot \boldsymbol{u}_s}. \tag{1.9}$$

The left-hand side of (1.9) is positive definite. But, in general, the sign of the individual terms on the right is indefinite. For instance, if $\overline{\boldsymbol{\tau}_s \cdot \boldsymbol{u}_s} > 0$, then it is impossible to discount the statically unstable possibility that $\Delta\bar{b} \leqslant 0$.

Most work on horizontal convection has taken $\boldsymbol{\tau}_s = 0$ so that $\Delta\bar{b}$ is positive, and then the strength of the kinetic energy source is bounded with $\varepsilon \leqslant \kappa b_{max}/H$. The literal statement of Sandström's theorem in Defant (1961) is contradicted by many experiments (Mullarney, Griffiths & Hughes 2004; Wang & Huang 2005; Coman, Griffiths & Hughes 2006). Nonetheless, the bound $\varepsilon \leqslant \kappa b_{max}/H$ provides a rigorous foundation for the thrust of Sandström's (1908) thermodynamic argument that non-uniform surface buoyancy alone cannot supply significant mechanical energy to the ocean circulation; see also McIntyre (2009) and Nycander (2010). A main point of interest in mechanically forced horizontal convection is that the system is relieved from this restrictive constraint on ε by additional source terms such as $\overline{\boldsymbol{\tau}_s \cdot \boldsymbol{u}_s}$.

2. A model of stressed horizontal convection

For the numerical simulations we consider a two-dimensional non-rotating Boussinesq fluid in a rectangular box, where the motion is in the (y, z)-plane, with the vertical coordinate $-H < z < 0$, and horizontal coordinate $0 < y < L$. Following Beardsley & Festa (1972) and Rossby (1998), we consider horizontal convection in the streamfunction–vorticity formulation with equations of motion

$$\nabla^2\psi_t + \psi_x\nabla^2\psi_z - \psi_z\nabla^2\psi_x = b_y + \nu\nabla^4\psi, \tag{2.1}$$

$$b_t + \psi_x b_z - \psi_z b_x = \kappa\nabla^2 b. \tag{2.2}$$

Above, the streamfunction is $\psi(y, z, t)$, and the incompressible velocity is $(v, w) = (-\psi_z, \psi_y)$. On the boundary of the domain $\psi = 0$.

Mechanical and buoyancy forcing is via the surface boundary conditions

$$b(y, 0, t) = b_{max}\cos^2\left(\frac{\pi y}{2L}\right), \quad \nu v_z(y, 0, t) = -\tau_{max}\sin\left(\frac{\pi y}{L}\right). \tag{2.3}$$

The surface buoyancy decreases smoothly and monotonically from $b = b_{max}$ at $y = 0$ to $b = 0$ at $y = L$. On the sidewalls and bottom there is no flux of buoyancy and no stress.

In (2.3), $\tau_{max} > 0$ so that the surface stress drives an anticlockwise circulation in the box. This is opposite in direction to the clockwise circulation forced by the surface buoyancy. We refer to this sense of mechanical forcing as 'thermally indirect', meaning that buoyant fluid near $y = 0$ is being pushed downwards by the stress, and the dense fluid at $y = L$ is elevated: e.g. Cessi (2007).

https://doi.org/10.1017/jfm.2011.514 Published online by Cambridge University Press

Thermally indirect forcing is relevant to the ocean: an east–west wind stress drives north–south Ekman surface flow, which is parallel to the main north–south temperature gradient, as in the two-dimensional system formulated above. In the thermally indirect case, the Ekman flow advects dense water over lighter water, triggering convection and creating weakly stratified 'mode waters' (Thomas 2005). The sub-polar oceans provide striking examples: the westerly wind stress drives an Ekman transport towards the equator in both hemispheres, producing basin-scale thermally indirect overturning.

2.1. *The control parameters*

As a dimensionless measure of the strength of the surface mechanical forcing, we introduce the stress parameter

$$S \stackrel{def}{=} \frac{\tau_{max} L^2}{\nu^2}. \tag{2.4}$$

The other three dimensionless parameters specifying this problem are familiar from earlier studies of unstressed horizontal convection. In the notation of Chiu-Webster, Hinch & Lister (2008), these are the aspect ratio, the horizontal Rayleigh number and the Prandtl number:

$$A \stackrel{def}{=} \frac{H}{L}, \quad R \stackrel{def}{=} \frac{b_{max} L^3}{\nu\kappa}, \quad \sigma \stackrel{def}{=} \frac{\nu}{\kappa}. \tag{2.5}$$

2.2. *Discussion of two representative solutions*

Figure 1 shows snapshots of two numerical solutions. The steady flow in figure 1(*a*) is unstressed horizontal convection. The main features in the upper panel, such as the thin surface boundary layer and the almost unstratified abyss, are familiar from many earlier studies. In this solution the average bottom buoyancy is $0.12 b_{max}$, which is considerably less than the mean surface buoyancy $b_{max}/2$.

Figure 1(*b*) shows the more complicated unsteady flow resulting from thermally indirect stress. It takes about half a vertical diffusion time, H^2/κ, to reach a statistically steady state. There is a shallow stress-driven anticlockwise cell and a second deep clockwise cell. Animations show that the deep cell is associated with pulses of dense fluid falling cyclically along the right-hand wall, beneath the densest part of the top surface. These pulses hit the bottom, turn the corner, and establish an unsteady bottom current flowing from $y = L$ towards $y = 0$. The flow in the upper left quadrant of the domain is steady.

A two-cell circulation is also evident in the relatively low-Rayleigh-number solutions shown in Figure 6 of Beardsley & Festa (1972). The two-cell circulation requires intermediate values of τ_{max} so that the stress is strong enough to reverse the surface velocity, $v_s = v(y, 0, t)$, but is not so strong as to overpower the buoyancy-driven circulation throughout the domain. A more quantitative estimate of the requisite τ_{max} is given below in the discussion surrounding (3.5).

In figure 1(*b*), v_s is in the same direction as the applied stress, so that the stress is doing positive work on the fluid. Using the surface stress in (2.3), the stress work in the power integral (1.9) is

$$\overline{\boldsymbol{\tau}_s \cdot \boldsymbol{u}_s} = -\tau_{max}\, \overline{v_s \sin(\pi y/L)}. \tag{2.6}$$

In figure 1(*b*) the abyssal fluid is more buoyant than in figure 1(*a*): stress increases the abyssal buoyancy by pumping buoyant fluid downwards in the upper cell. In fact, the average bottom buoyancy is $0.55 b_{max}$, so that in (1.9) $\Delta\bar{b} = -0.05 b_{max}$; because

https://doi.org/10.1017/jfm.2011.514 Published online by Cambridge University Press

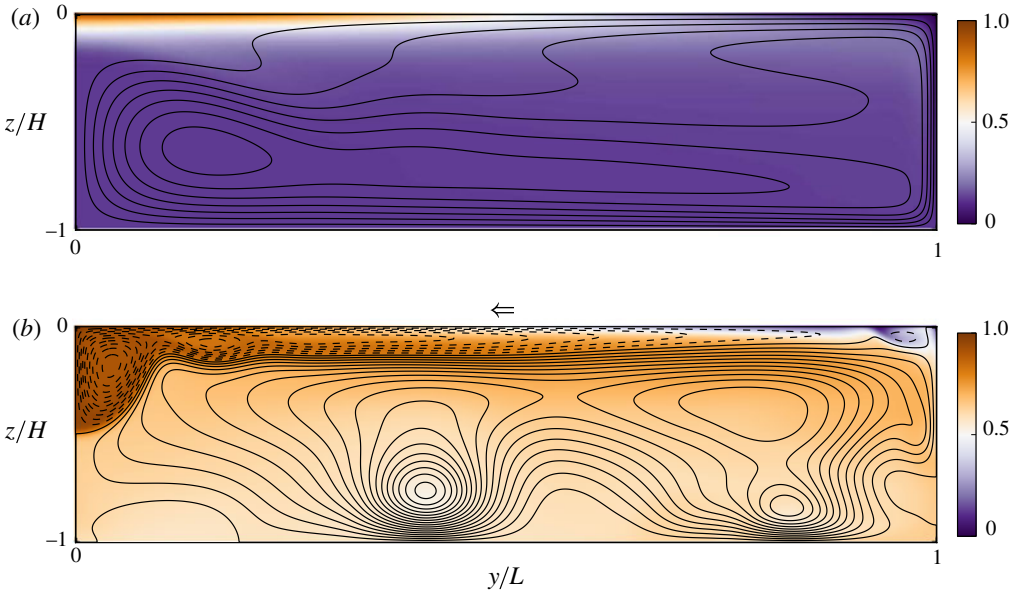


FIGURE 1. Two snapshots of the buoyancy field (shading) and the streamfunction ψ. Solid contours are $\psi > 0$, dashed contours are $\psi < 0$; the contour interval is $\Delta\psi = 10\kappa$. (*a*) Steady solution at $t = H^2/\kappa$ with with no stress, i.e. the stress parameter S defined in (2.4) is $S = 0$. (*b*) Unsteady solution at $t = 1.3H^2/\kappa$ with $S = 1.1 \times 10^6$. The direction of the applied surface stress is indicated by ⇐. These solutions have $R = 64 \times 10^7$, $A = 1/4$ and $\sigma = 1$. (*a*) $S_\delta = 0$, (*b*) $S_\delta = 5.8$.

$\Delta\bar{b} < 0$, energy is being converted from kinetic to potential energy. Thus the positive $\overline{\boldsymbol{\tau}_s \cdot \boldsymbol{u}_s}$ balances the dissipation ε, and $\overline{\boldsymbol{\tau}_s \cdot \boldsymbol{u}_s}$ also provides the net production of potential energy required by $\Delta\bar{b} < 0$.

Figure 1(*a*) shows the unstressed case, and figure 1(*b*) shows a case with moderately strong stress in which there is a top-to-bottom inversion of the density. Figure 2(*a*), showing the horizontally averaged buoyancy $\bar{b}(z)$, summarizes a suite of solutions in which τ_{max} varies between the extremes shown in figure 1. The abyssal buoyancy increases monotonically with τ_{max}; very small τ_{max} produces small density inversions confined to the upper cell. At a particular value of τ_{max} – which is less than the value in figure 1(*b*) – the average bottom buoyancy is equal to $b_{max}/2$, so that $\Delta\bar{b} = 0$.

If τ_{max} is increased past the value at which $\Delta\bar{b} = 0$, as it is in figure 1(*b*), then there is a top-to-bottom density inversion, even though the squared buoyancy frequency,

$$N^2 \stackrel{def}{=} \bar{b}_z, \tag{2.7}$$

is negative only in the relatively small upper cell: see figure 2(*b*).

Increases in τ_{max} lead to the point where the buoyant 'blob' evident in the top left corner of figure 1(*b*) is pushed down to the bottom. At this threshold, the lower thermally direct cell collapses and the circulation is thermally indirect everywhere, i.e. the stress wins. Except at the top boundary, where a non-uniform buoyancy is prescribed, the buoyancy is homogenized to around $0.65b_{max}$. In this mechanically dominated regime the buoyancy is almost a passive scalar and the top boundary layer

https://doi.org/10.1017/jfm.2011.514 Published online by Cambridge University Press

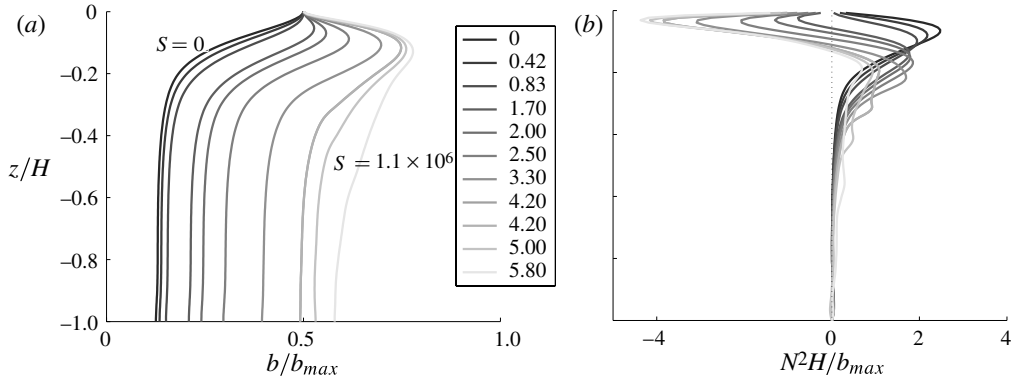


FIGURE 2. (*a*) Horizontally averaged buoyancy profiles, $\bar{b}(z)$, (*b*) the buoyancy frequency in (2.7). The Rayleigh number is $R = 64 \times 10^7$ with various values of S. The end points $S = 0$ and 9.6×10^5 are the solutions in figure 1. The parameter in the legend is S_δ defined in (3.5).

becomes very thin, and our resolution is no longer sufficient. Figure 1(*b*) shows the largest τ_{max} at which we can afford the requisite boundary-layer resolution.

The stress work $\overline{\boldsymbol{\tau}_s \cdot \boldsymbol{u}_s}$ has an interesting dependence on τ_{max}. Small τ_{max} does not manage to reverse the sign of v_s, and therefore the surface flow is against the direction of the stress, so that $\overline{\boldsymbol{\tau}_s \cdot \boldsymbol{u}_s} < 0$. That is, the first effect of thermally indirect surface stress is to make the circulation weaker. However, increasing τ_{max} eventually reverses v_s so that $\overline{\boldsymbol{\tau}_s \cdot \boldsymbol{u}_s}$ becomes positive. The transition can be identified precisely by the condition that $\overline{\boldsymbol{\tau}_s \cdot \boldsymbol{u}_s} = 0$, which happens at a smaller value of τ_{max} than the full-depth inversion signalled by $\Delta\bar{b} = 0$. In § 3 we use a scaling arguments to more quantitatively delineate the occurrence of the two transitions $\overline{\boldsymbol{\tau}_s \cdot \boldsymbol{u}_s} = 0$ and $\Delta\bar{b} = 0$.

2.3. *Remarks on the numerical solution*

The system in (2.1) and (2.2) is solved using the same code as Paparella & Young (2002). The numerical representation of vorticity and temperature is a second-order finite difference in space with a staggered grid. The Jacobian terms are discretized with the Arakawa Jacobian formulation (Arakawa 1966) and the elliptic problem for the streamfunction, with a given vorticity, is solved with a multigrid method (Briggs 1987). The Laplacian terms are based on the DuFort–Frankel discretization (DuFort & Frankel 1953), which is a stable and relatively accurate scheme as long as the time step obeys the Courant–Friedrichs–Lewy condition (CFL) condition. We adjusted the time step so that the CFL number is less than 0.05. When the spatial resolution appears to be too coarse for the features in the simulated flow, runs at double the resolution were performed in order to achieve a more accurate solution; the highest spatial resolution we could afford was 1024×256. Unfortunately the simulations at $R = 64 \times 10^8$ must be treated with caution because resolutions less than 1024×256 do not adequately resolve the small-scale structures in the flow, and we cannot afford to substantially increase the resolution beyond 1024×256. At the less demanding setting $R = 64 \times 10^7$, we compare averaged quantities from 512×128 solutions with those from solutions at 1024×256. Global averages, such as $\langle wb \rangle$, $\overline{\boldsymbol{\tau}_s \cdot \boldsymbol{u}_s}$ and ε, change by less than 3 %. We do not present the results with error estimates: globally averaged quantities have error estimates in the order of a few per cent. Typically, the unstressed simulations reach a steady state, or statistically steady state, within one half of a

https://doi.org/10.1017/jfm.2011.514 Published online by Cambridge University Press

vertical diffusion time, H^2/κ. We integrated all solutions for at least one full diffusion time.

3. Scaling arguments

3.1. *Rossby scaling*

In the unstressed case, with $S = 0$, the scaling argument of Rossby (1965) provides a satisfactory condensation of all known numerical solutions: e.g. Siggers, Kerswell & Balmforth (2004), Chiu-Webster *et al.* (2008) and Ilicak & Vallis (2011). The first step in Rossby's argument is assuming that the typical vertical variation of buoyancy within the surface boundary layer is b_{max}. If the dominant boundary-layer balance in (2.1) is between b_y and vertical diffusion of vorticity, $\nu\psi_{zzzz}$, then one has

$$V \sim \frac{b_{max}\delta^3}{\nu L}, \tag{3.1}$$

where δ is the boundary-layer thickness, and V is the typical horizontal velocity in the boundary layer. A second scaling relation comes from a dominant balance in the buoyancy equation (2.2) between the advective terms, which scale as Vb_{max}/L, and the vertical diffusion scaling as $\kappa b_{max}/\delta^2$, leading to

$$V \sim \frac{L\kappa}{\delta^2}. \tag{3.2}$$

From (3.1) and (3.2), Rossby (1965) obtains the boundary-layer thickness

$$\delta \sim \frac{L}{R^{1/5}}, \tag{3.3}$$

and the boundary-layer velocity

$$V \sim \frac{\kappa}{L}R^{2/5}. \tag{3.4}$$

3.2. *A scaling regime for stressed horizontal convection*

In order for the surface stress to be competitive with the buoyancy forcing, one must have $\tau_{max} \sim \nu V/\delta$, so that the magnitude of the imposed surface stress is comparable to the stress across Rossby's purely buoyancy boundary layer. In terms of control parameters, this condition is $S \sim \sigma^{-1}R^{3/5}$. This motivates the introduction of the non-dimensional ratio

$$S_\delta \overset{def}{=} \frac{\sigma S}{R^{3/5}}. \tag{3.5}$$

If $S_\delta \ll 1$, then the stress τ_{max} is only a weak perturbation of the buoyancy-driven boundary layer, while if $S_\delta \gg 1$, then the flow is strongly mechanically forced. Notice that the solutions summarized in figure 2 have S_δ of order unity.

The scaling relations in (3.3) and (3.4) motivate the hypothesis that in the distinguished limit $R \to \infty$ and $S \to \infty$, with σ, A and S_δ fixed, the boundary-layer thickness and velocity are given by

$$\delta = LR^{-1/5}\,\delta_*(\sigma, S_\delta, A), \qquad V = \kappa L^{-1}R^{2/5}\,V_*(\sigma, S_\delta, A), \tag{3.6}$$

where δ_* and V_* are non-dimensional functions. In this sense Rossby scaling applies to stressed horizontal convection and S_δ provides an objective means of comparing the strength of the stress forcing with that of the buoyancy forcing. We present numerical evidence in support of this hypothesis in § 4.

https://doi.org/10.1017/jfm.2011.514 Published online by Cambridge University Press

3.3. *Static instability in the upper boundary layer*

In the solutions shown in figures 1 and 2, the stress is dragging dense fluid over light and inducing a statically inverted buoyancy field. This density inversion can remain stable if the local vertical Rayleigh number within Rossby's boundary layer is sufficiently small. One can estimate the relevant boundary-layer Rayleigh number as $b_{max}\delta^3/\nu\kappa \sim R^{2/5}$. This motivates the definition of a boundary-layer Rayleigh number

$$R_\delta \stackrel{def}{=} R^{2/5}. \tag{3.7}$$

If the mechanical stress is thermally indirect, with $S_\delta = 0(1)$, and R is increased sufficiently, then experience with Rayleigh–Bénard convection suggests that the static inversion should trigger convection once $R_\delta > 10^3$. The solutions at $R = 64 \times 10^7$ and 64×10^8 have $R_\delta = 3330$ and 8365 respectively, yet there is no indication of convection within the boundary layer in any of our simulations. Either $R_\delta = 8365$ is too small, or the shear across the boundary layer, $V/\delta \sim \kappa R^{3/5}/L^2$, is suppressing convection.

In a three-dimensional situation, rolls parallel to the y-axis, with overturning orthogonal to the plane of figure 1, would be unaffected by the boundary-layer shear v_z, and are therefore the most likely mode of instability; e.g. as in Gayen & Sarkar (2010). We proceed by considering only the two-dimensional configuration.

To assess the possible role of boundary-layer shear in the regime with

$$S_\delta = O(1), \tag{3.8}$$

we compare the shear time scale with the time it takes a parcel to fall through the boundary-layer density inversion. The shear time scale can be estimated as either δ/V or, from the boundary condition (2.3), as ν/τ_{max}. The requirement that these two estimates of the shear time have the same magnitude is our starting point in (3.8). If the boundary-layer buoyancy inversion is of order b_{max}, and occurs over a distance δ, then the time it takes a heavy parcel to fall to its neutral level is $\sqrt{\delta/b_{max}}$. Thus we obtain a non-dimensional ratio

$$\frac{\text{fall time through } \delta}{\text{shear time scale}} = \sqrt{\frac{\delta}{b_{max}}}\frac{\tau_{max}}{\nu} = \frac{S_\delta}{\sqrt{\sigma}}. \tag{3.9}$$

Convection might occur if the parameter above is sufficiently small, i.e. if parcels can release potential energy by falling through the boundary layer, before being sheared into oblivion. On the other hand, to invert the boundary-layer buoyancy requires that S_δ be sufficiently large. With $\sigma = 1$ these two requirements cannot both be satisfied; that is, if the shear is strong enough to invert the boundary-layer buoyancy, it is also strong enough to stabilize the inversion by preventing convective overturning in the plane of figure 1.

These considerations led us to obtain solutions with $\sigma = 10$ so that S_δ can be significantly larger than one, while $S_\delta/\sqrt{\sigma}$ is less than one. Then, according to (3.9), the inverted boundary-layer buoyancy might result in convection within the boundary layer. Figure 3 shows the three $\sigma = 10$ solutions, and indeed unsteady boundary-layer convection is evident in figure 3(*b*).

It is remarkable that boundary-layer convection occurs only in the intermediate case in figure 3(*b*): the other solutions in figure 3 are steady. In panel (*a*) the stress is weak and the thermally indirect upper cell is undeveloped. Consequently the buoyancy inversion is not strong enough to result in boundary-layer convection. In panel (*c*) the strong stress produces a complex, but steady, pattern with two co-rotating cells within the boundary layer. Although the buoyancy inversion is strong, the flow in panel (*c*) is steady.

https://doi.org/10.1017/jfm.2011.514 Published online by Cambridge University Press

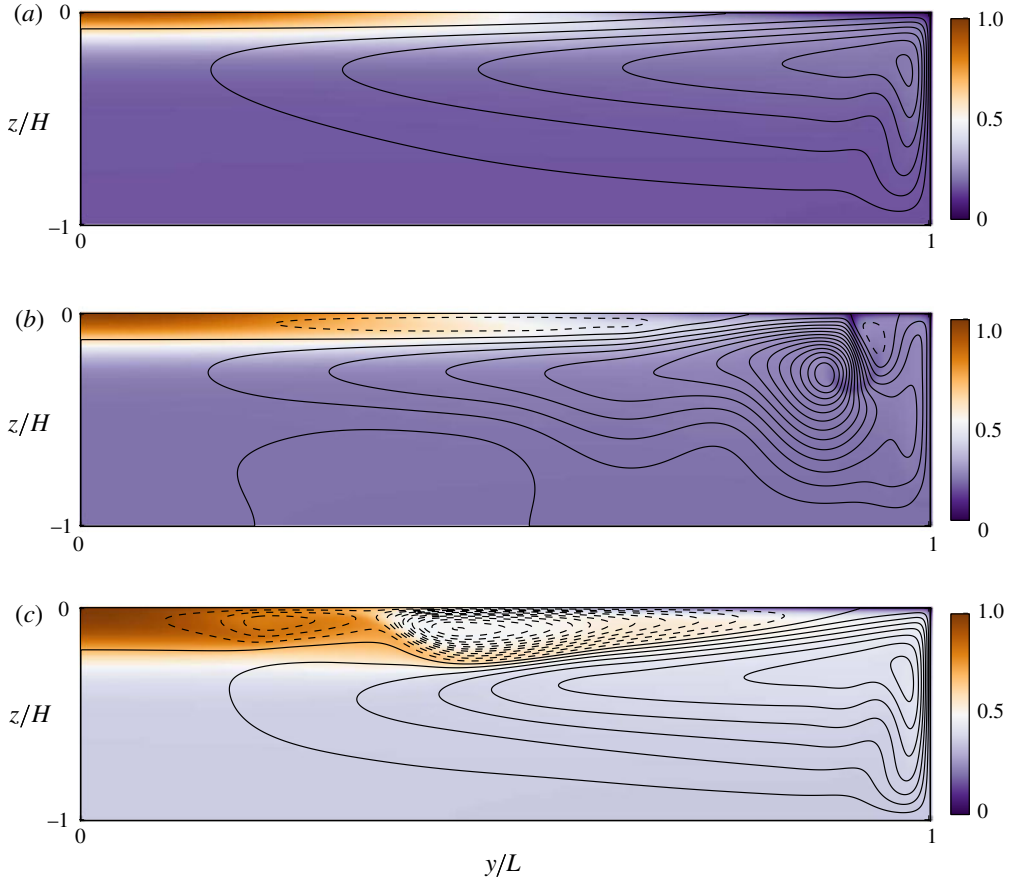


FIGURE 3. Buoyancy and streamfunction of three solutions with $R = 64 \times 10^7$, $\sigma = 10$ and $A = 4$. The parameter in (3.9) is $S_\delta/\sqrt{\sigma} = 0.39$ (*a*), 0.65 (*b*) and 1.05 (*c*). Solid contours are $\psi > 0$, dashed contours are $\psi < 0$; the contour interval is $\Delta\psi = 10\kappa$.

Animations of the solution in figure 3(*b*) show that the thermally indirect flow in the upper cell produces an inversion which steadily becomes stronger until convective plumes suddenly appear and release the potential energy. Discharging the top-heavy inversion and quenching the convection requires several plumes to form and then fall through the boundary layer. As shown by the time series of potential energy in figure 4, this process repeats cyclically so that there are epochs of convection followed by epochs during which the inversion is re-established: see figure 5 (which shows only the top right corner of the domain). Both stages are slow: a gradual build-up of the stress-driven inversion, followed by a slow discharge via a sequence of plumes.

4. Verification of the scaling

With the Rossby scaling relations we can collapse the results of computations in the range $64 \times 10^5 \leqslant R \leqslant 64 \times 10^8$ and $0 < S_\delta < 5.8$. In figure 6(*a*) we confirm the scaling argument from § 3 by showing that the vertical coordinate z/δ collapses $\bar{b}(z)$ profiles at fixed values of S_δ.

https://doi.org/10.1017/jfm.2011.514 Published online by Cambridge University Press

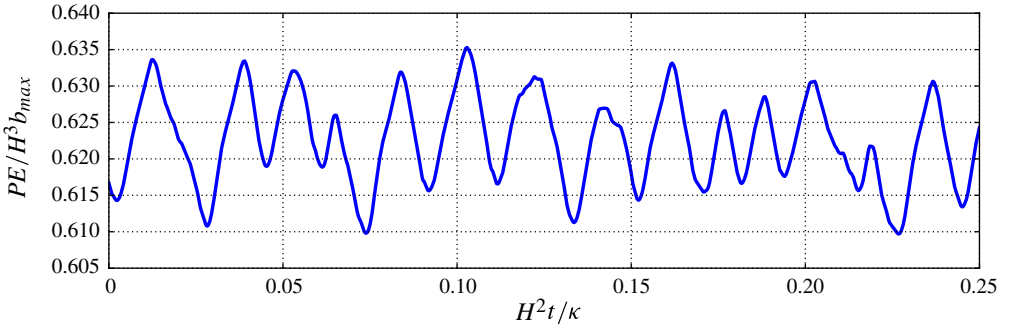


FIGURE 4. (Colour online available at journals.cambridge.org/flm) A time series of potential energy, $PE(t) = -\int zb\,\mathrm{d}V$, for the solution shown in figure 3(*b*).

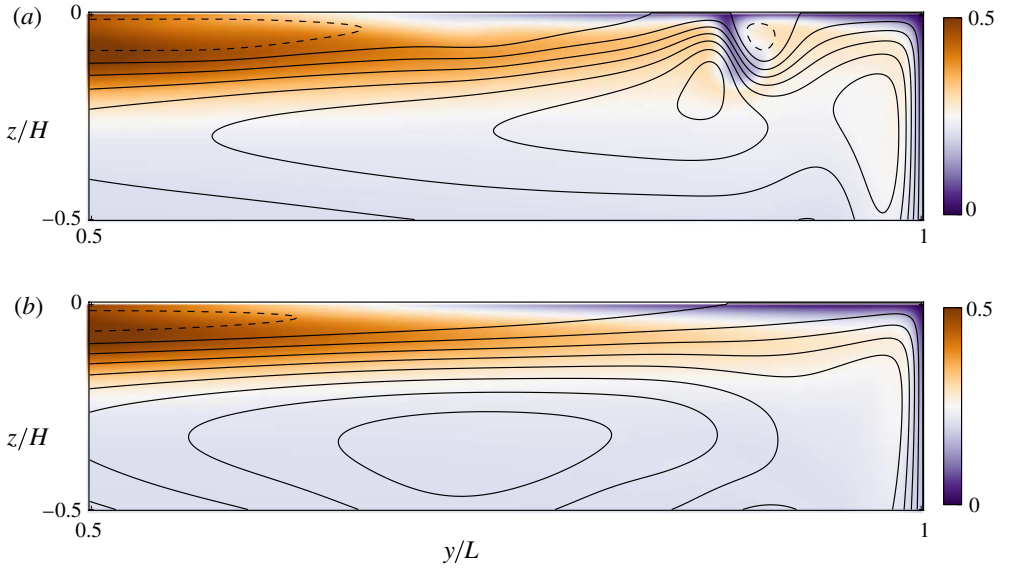


FIGURE 5. (*a*) Snapshot of the solution at the first peak of the potential-energy time series in figure 4. (*b*) Snapshot at the minimum *PE* immediately after the snapshot in (*a*). The top right quarter of the domain in figure 4 is shown, and the colour scale has been changed to better show structure in the boundary layer. Eight plumes fall through the boundary layer between the two snapshots. Solid contours are $\psi > 0$, dashed contours are $\psi < 0$; the contour interval is $\Delta\psi = 10\kappa$.

Figure 6(*b*) shows the horizontally averaged bottom buoyancy $\bar{b}(-H)$; the bottom buoyancy increases monotonically with increasing S at fixed R. At fixed S_δ, $\bar{b}(-H)$ decreases slowly with increasing R and seems to approach a non-zero constant as $R \to \infty$; we have not been able to obtain a satisfactory scaling for the dependence of $\bar{b}(-H)/b_{max}$ on R. In figure 6(*b*) we see that $\Delta\bar{b} = 0.5b_{max}$ (i.e. $\Delta\bar{b} = 0$) when S_δ is in the range four to five (the value depends on R). In the sequence with $R = 64 \times 10^8$, the flow is weakly unsteady for all solutions with $S_\delta \geqslant 3$ and $\bar{b}(-H)$ is never larger than the mean top buoyancy $\bar{b}(0) = 0.5b_{max}$. This leads us to speculate that as $R \to \infty$, with

https://doi.org/10.1017/jfm.2011.514 Published online by Cambridge University Press

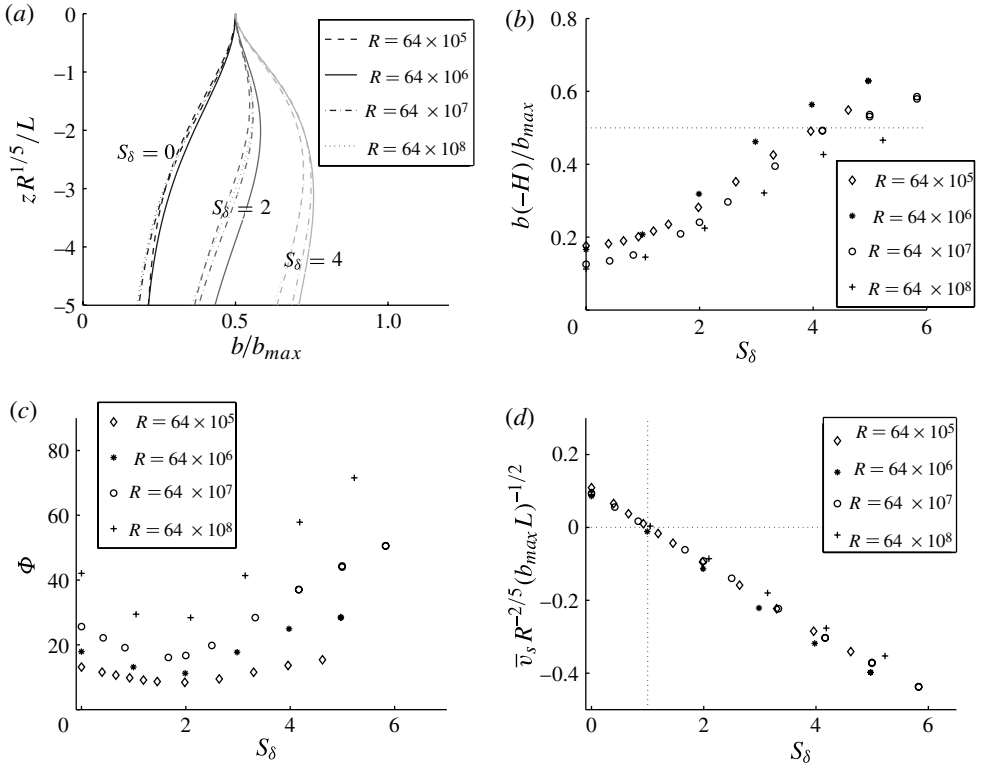


FIGURE 6. Solutions with $\sigma = 1$. (*a*) Horizontally averaged buoyancy $\bar{b}$ against z/δ. (*b*) Horizontally averaged buoyancy at the bottom $z = -H$. (*c*) The index Φ in (4.1). (*d*) Averaged surface velocity $\bar{v}_s$. Double markers at the same S_δ correspond to results at different resolution.

S_δ fixed at a largish value such as five or six, the bottom buoyancy $\bar{b}(-H)$ saturates at $b_{max}/2$, so that $\Delta\bar{b} = 0$. In other words, at very high horizontal Rayleigh numbers it is impossible for surface stress to coerce a top-to-bottom density inversion. Via (1.8), this scenario also entails a shutdown of the conversion between potential energy and kinetic energy.

As an index of the strength of horizontal convective heat transport and diapycnal mixing, Paparella & Young (2002) introduced

$$\Phi \stackrel{def}{=} \frac{\langle \boldsymbol{\nabla} b \cdot \boldsymbol{\nabla} b \rangle}{\langle \boldsymbol{\nabla} c \cdot \boldsymbol{\nabla} c \rangle}, \tag{4.1}$$

where $c(\boldsymbol{x})$ is the solution of the conduction problem $\nabla^2 c = 0$, with c satisfying the same boundary conditions as b, i.e. $c = b$ at the top surface and the normal derivative of c is zero at the other boundaries. For the unsteady solutions, temporal pulsations in Φ are removed by averaging over half a diffusive time.

Figure 6(*c*) shows Φ for various R as a function of S_δ. For all R there is an initial decrease in Φ for increasing S_δ. The weakest horizontal convection, as indicated by the minimum in Φ, is at $S_\delta \approx 2$. Thereafter Φ increases with S_δ. For small stress the surface velocity is determined by the buoyancy forcing and is therefore against the wind, so that $\overline{\boldsymbol{\tau}_s \cdot \boldsymbol{u}_s} < 0$. In this regime the surface stress is working against the fluid and slowing down the circulation. But if the stress is strong enough to reverse the sign

https://doi.org/10.1017/jfm.2011.514 Published online by Cambridge University Press

of the surface velocity, then the stress work $\overline{\boldsymbol{\tau}_s \cdot \boldsymbol{u}_s}$ becomes positive; that is, if the surface flow is downwind then the surface stress is doing work on the fluid. In this wind-powered regime, Φ increases with stress.

The behaviour observed in both $\bar{b}(-H)$ and Φ is qualitatively similar to the $R = 10^4$ solutions shown in figures 7 and 9 of Beardsley & Festa (1972). Using kinetic energy as an index, Beardsley & Festa (1972) also remarked on the non-monotonic dependence of the strength of the circulation on the surface stress.

Strong evidence supporting the earlier scaling arguments is provided by the variation of the surface velocity v_s with the surface stress. In figure 6(*d*) we plot the scaled mean surface velocity $R^{-2/5}\bar{v}_s$ against S_δ: there is good collapse of the data and $\bar{v}_s$ changes sign at $S_\delta \approx 1$ for all R.

5. Conclusion and discussion

One motivation for studying stressed horizontal convection is to better understand the role of mechanical forcing in the power integral (1.9). Here, and in Ilicak & Vallis (2011), a surface stress is applied to the system. Tailleux & Rouleau (2010) use an interior body force to inject mechanical energy, and in a laboratory study Whitehead & Wang (2008) use three-dimensional grid-generated turbulence to supply mechanical energy to a horizontal convective system. In the same vein, Dewar *et al.* (2006) suggest that the locomotion of marine organisms might supply significant mixing energy to the interior ocean. These are all strategies for avoiding the constraint $\varepsilon < \kappa b_{max}/H$ by adding a term analogous to the stress work $\overline{\boldsymbol{\tau}_s \cdot \boldsymbol{u}_s}$ to the right of the power integral (1.9). We have shown that sufficiently strong mechanical forcing leads to an increase in the strength of the circulation, as indicated for example by the ultimate increase in Φ with S_δ in figure 6(*c*).

However, the power integral (1.9) is only a single relation between globally averaged quantities, and thus cannot strongly constrain the phenomenology of horizontal convection throughout the four-dimensional parameter space (R, S, σ, A); for example, the circulations in figure 1 (with $\sigma = 1$) and figure 3 (with $\sigma = 10$) are quite different, even in the cases with no surface stress. Ilicak & Vallis (2011) provide further examples of the diverse phenomenology of horizontal convection. A characteristic feature of the steady surface stress investigated in this paper is the two-celled circulation shown in figures 1 and 3. The shallow, thermally indirect cell is evident even in the early study of Beardsley & Festa (1972). The generalized Rossby scaling proposed in (3.6) proves very useful in condensing the results in this two-cell regime.

Modern descriptive studies, based on strict use of isopycnal analysis, emphasize that the Earth's oceans have a multi-cell overturning structure, and that the shallow wind-driven cell, which has the greatest vertical temperature differences, is responsible for most of the heat transport (Talley 2003). We must cautiously interpret the oceanographic application of the very idealized problem of stressed horizontal convection (see below). But we cannot resist remarking that the two-cell overturning pattern in our solutions is a feature of the ocean circulation, and probably for the same reason: stress forcing drives the shallow cell, while the deeper cell is associated with bottom-water formation and upwelling.

Further regarding the oceanographic implications of these results, the problem of horizontal convection can be considered an idealized and instructive thought experiment applying to the 'Sandström ocean' rather than the 'real ocean'. Like the real ocean, Sandström's ocean is forced by stress and buoyancy at the top surface,

https://doi.org/10.1017/jfm.2011.514 Published online by Cambridge University Press

and one can estimate the Rossby scales in (3.3) and (3.4) using oceanographic parameter values (Stern 1975). Suppose that $b_{max} = 5 \times 10^{-2}$ m s^{-2}, corresponding to a temperature difference of 25 K and a thermal expansion coefficient of 2×10^{-4} K^{-1}. For the horizontal dimension, use the planetary scale $L = 10^7$ m, and molecular parameters $\kappa = 10^{-7}$ m^2 s^{-1} and $\nu = 10\kappa$. Then $R = 5 \times 10^{32}$, and the Rossby boundary-layer scales are $\delta = 2.9$ m and $V = 0.12$ m s^{-1}. If instead one uses eddy diffusion and viscosity with $\nu = \kappa = 10^{-4}$ m^2 s^{-1} (without specifying the energy source required to support this mixing), then the Rayleigh number drops to $R = 5 \times 10^{27}$, and the implied Rossby scales are $\delta = 29$ m and $V = 1.2$ m s^{-1}. It is a remarkable prediction of Rossby scaling that decreasing the Rayleigh number by increasing the diffusivity κ results in a larger V.

Rather small values of τ_{max} result in $S_\delta = O(1)$. For example, using the numerical values corresponding to $R = 5 \times 10^{32}$ above, a typical ocean wind stress of $\rho_0 \tau_{max} = 0.1$ N m^{-2} gives $S = 10^{22}$ and $S_\delta = 2400$. If instead one uses eddy viscosity and diffusivity, so that $R = 5 \times 10^{27}$, then $S = 10^{18}$ and $S_\delta = 24$. In both cases our computations indicate that the flow would consist of a single, thermally indirect cell. That is, with $S_\delta \gg 1$ (and 24 is large enough), the circulation is a single-cell, thermally indirect, stress-driven cavity flow; the buoyancy is almost a passive scalar.

The numerical estimates above suppose that Rossby's scaling remains valid in the distinguished limit $R \to \infty$ and $S \to \infty$, with S_δ fixed and order unity. We speculate that three-dimensional effects and turbulence (energized by the surface stress) destroy Rossby scaling once R is sufficiently large. With applied surface stress, either steady or oscillatory, there is no energetic principle preventing the generation of shallow turbulence, vertical radiation of internal gravity waves, wave breaking, abyssal mixing and the development of deep stratification. Presumably this chain of events, which may require three-dimensional dynamics (Scotti & White 2011), will destroy the Rossby scaling so that the boundary layer is realistically thick and the abyss is significantly stratified, even in Sandström's ocean. But with $R = O(10^8)$ we have not been able to access this hypothetical regime, in which Sandström's ocean is self-mixing and the abyssal stratification is significant; see also Ilicak & Vallis (2011).

For the unstressed case, Hughes *et al.* (2007) have formulated a 'recycling-box' model of the very large Rayleigh number regime. Recycling-box solutions, using oceanic parameter values, such as an eddy diffusivity $\kappa = 10^{-5}$ m^2 s^{-1}, have a boundary-layer thickness comparable to the depth of the ocean. Thus recycling-box solutions predict that the boundary layer is much thicker than that of Rossby. It is not clear how, or if, Rossby scaling gives way as to the different scaling of Hughes *et al.* (2007) as $R \to \infty$. Certainly the Prandtl number σ should have some role in this issue. Thus a main open question is finding a large-R replacement for Rossby scaling, and then employing this hypothetical large-R scaling to objectively compare the strength of buoyancy and stress forcing.

Acknowledgements

This work was supported by the National Science Foundation under OCE-1057838. We thank R. Barkan, R. Griffiths, A. Hogg, K. Matusik, J. Nycander, A. Scotti, K. Stewart, R. Tailleux, G. Vallis and K. Winters for helpful discussion of this problem.

https://doi.org/10.1017/jfm.2011.514 Published online by Cambridge University Press

REFERENCES

ARAKAWA, A. 1966 Computational design for long-term numerical integration of the equations of fluid motion: two-dimensional incompressible flow. Part I. *J. Comput. Phys.* **1** (1), 119–143.

BEARDSLEY, R. C. & FESTA, J. F. 1972 A numerical model of convection driven by a surface stress and non-uniform horizontal heating. *J. Phys. Oceanogr.* **2** (4), 444–455.

BRIGGS, W. 1987 *A Multigrid Tutorial*. SIAM.

CESSI, P. 2007 Regimes of thermohaline scaling: the interaction of wind stress and surface buoyancy. *J. Phys. Oceanogr.* **37**, 2009–2021.

CHIU-WEBSTER, S., HINCH, E. J. & LISTER, J. R. 2008 Very viscous horizontal convection. *J. Fluid Mech.* **611**, 395–426.

COMAN, M. A., GRIFFITHS, R. W. & HUGHES, G. O. 2006 Sandström's experiments revisited. *J. Mar. Res.* **64** (14), 783–796.

DEFANT, A. 1961 *Physical Oceanography: vol. I.* Macmillan.

DEWAR, W. K., BINGHAM, R. J., IVERSON, R. L., NOWACEK, D. P., LAURENT, L. C. S. & WIEBE, P. H. 2006 Does the marine biosphere mix the ocean? *J. Mar. Res.* **64** (21), 541–561.

DUFORT, E. C. & FRANKEL, S. P. 1953 Stability conditions in the numerical treatment of parabolic differential equations. *Math. Tables Other Aids Comput.* **7** (43), 135–152.

GAYEN, B. & SARKAR, S. 2010 Turbulence during the generation of internal tide on a critical slope. *Phys. Rev. Lett.* **104**, 218502.

HUGHES, G. O. & GRIFFITHS, R. W. 2008 Horizontal convection. *Annu. Rev. Fluid Mech.* **40**, 185–208.

HUGHES, G., GRIFFITH, R., MULLARNEY, J. & PETERSON, W. 2007 A theoretical model for horizontal convection at high Rayleigh number. *J. Fluid Mech.* **581**, 251–276.

HUGHES, G. O., HOGG, A. M. & GRIFFITHS, R. W. 2009 Available potential energy and irreversible mixing in the meridional overturning circulation. *J. Phys. Oceanogr.* **39**, 3130–3146.

ILICAK, M. & VALLIS, G. K. 2011 Simulations and scaling of horizontal convection. *Tellus* (submitted).

KUHLBRODT, T. 2008 On Sandström's inferences from his tank experiments: a hundred years later. *Tellus* A **60** (5), 819–836.

MCINTYRE, M. E. 2009 On spontaneous imbalance and ocean turbulence: generalizations of the Paparella–Young epsilon theorem. In *Turbulence in the Atmosphere and Oceans* (ed. D. G. Dritschel). *Proc. Intl. IUTAM/Newton Workshop held 8–12 December 2008*, pp. 3–15. Springer.

MULLARNEY, J., GRIFFITHS, R. W. & HUGHES, G. O. 2004 Convection driven by differential heating at a horizontal boundary. *J. Fluid Mech.* **516**, 181–209.

MUNK, W. & WUNSCH, C. I. 1998 Abyssal recipes. Part II. Energetics of tidal and wind mixing. *Deep Sea Res.* I **45** (12), 1977–2010.

NYCANDER, J. 2010 Horizontal convection with a nonlinear equation of state: generalization of a theorem of Paparella and Young. *Tellus* A **62** (2), 134–137.

PAPARELLA, F. & YOUNG, W. R. 2002 Horizontal convection is non-turbulent. *J. Fluid Mech.* **466**, 205–214.

ROSSBY, H. T. 1965 On thermal convection driven by non-uniform heating from below: an experimental study. *Deep Sea Res. Oceanogr. Abst.* **12** (1), 9–10 IN9–IN14, 11–16.

ROSSBY, H. T. 1998 Numerical experiments with a fluid heated non-uniformly from below. *Tellus* A **50** (2), 242–257.

SANDSTRÖM, J. W. 1908 Dynamische Versuche mit Meerwasser. *Ann. Hydrogr. Mar. Met.* **36**, 6–23.

SCOTTI, A. & WHITE, B. 2011 Is horizontal convection really non-turbulent? *Geophys. Res. Lett.* (accepted).

SIGGERS, J. H., KERSWELL, R. R. & BALMFORTH, N. J. 2004 Bounds on horizontal convection. *J. Fluid Mech.* **517**, 55–70.

STERN, M. E. 1975 *Ocean Circulation Physics*. Academic Press.

https://doi.org/10.1017/jfm.2011.514 Published online by Cambridge University Press

TAILLEUX, R. 2009 On the energetics of stratified turbulent mixing, irreversible thermodynamics, Boussinesq models, and the ocean heat engine controversy. *J. Fluid Mech.* **638**, 339–382.

TAILLEUX, R. & ROULEAU, L. 2010 The effect of mechanical stirring on horizontal convection. *Tellus* A **62** (2), 138–153.

TALLEY, L. D. 2003 Shallow, intermediate and deep overturning components of the global heat budget. *J. Phys. Oceanogr.* **33**, 530–560.

THOMAS, L. 2005 Destruction of potential vorticity by fronts. *J. Phys. Oceanogr.* **35**, 2457–2466.

WANG, W. & HUANG, R. X. 2005 An experimental study on thermal convection driven by horizontal differential heating. *J. Fluid Mech.* **540**, 49–73.

WHITEHEAD, J. A. & WANG, W. 2008 A laboratory model of vertical ocean circulation driven by mixing. *J. Phys. Oceanogr.* **39**, 1091–1106.

WINTERS, K. B. & YOUNG, W. R. 2009 Available potential energy and buoyancy variance in horizontal convection. *J. Fluid Mech.* **629**, 221–230.

https://doi.org/10.1017/jfm.2011.514 Published online by Cambridge University Press